JOURNAL OF GEOPHYSICAL RESEARCH, VOL. 111, A09309, doi:10.1029/2005JA011197, 2006



# Characterization of exceptionally strong mesospheric wave events using all-sky and zenith airglow observations

Steven M. Smith,[1] Jürgen Scheer,[2] Esteban R. Reisin,[2] Jeffrey Baumgardner,[1] and Michael Mendillo[1]

Received 18 April 2005; revised 28 May 2006; accepted 5 June 2006; published 19 September 2006.

[1] Two unusually clear mesospheric gravity wave events were observed by the Boston University all-sky imager and the Argentine airglow spectrometer on two consecutive nights at the El Leoncito Observatory, Argentina (31.8°S, 69.3°W), during August 2001. Both events exhibited brightness amplitudes an order of magnitude above typical values. The first event had the appearance of a large-amplitude (>60% in OH(6-2), 22% in $O_2$, and 37% in O($^1$S) emissions (peak to peak), compared to 1–5% typically), upward propagating gravity wave with pronounced nonlinear behavior. The waves also showed noticeably curved wavefronts, indicating that they had originated from a relatively small source region within ~180 km of El Leoncito. Estimates of the vertical flux of horizontal energy and momentum for the wave event in the OH and $O_2$ emissions were very large compared to typical values, and they also indicated a high degree of flux divergence over the nominal 8 km altitude between the two layers. The second event occurred on the following night and exhibited a frontal morphology and behavior consistent with an internal ducted gravity wave showing nonlinear behavior akin to a mesospheric bore. The disturbance also had several interesting characteristics; in particular, the propagation speed decreased during its passage across the sky. In addition, a strong vertical temperature gradient due to the semidiurnal tide appeared to influence the occurrence of the bore event.

**Citation:** Smith, S. M., J. Scheer, E. R. Reisin, J. Baumgardner, and M. Mendillo (2006), Characterization of exceptionally strong mesospheric wave events using all-sky and zenith airglow observations, *J. Geophys. Res.*, *111*, A09309, doi:10.1029/2005JA011197.

## 1. Introduction

[2] The advent of modern bare CCD detectors [e.g., *Taylor et al.*, 1995a; *Wu and Killeen*, 1996; *Hecht et al.*, 1997; *Swenson et al.*, 1999; *Smith et al.*, 2000] has made quasi-monochromatic (QM) gravity waves a ubiquitous feature in all-sky images of the mesospheric nightglow. They are usually a very faint and subtle phenomenon and so are rarely recorded in images obtained with the older and less sensitive intensified CCD (ICCDs) detectors. Yet, two strong wave events were recorded in the OH and O($^1$S) emissions with the Boston University ICCD all-sky imager at the El Leoncito Observatory (31.8°S, 69.3°W) on the consecutive nights of 22 and 23 August 2001 (we use a date notation valid after midnight). The events were also recorded in the OH(6-2) and $O_2b(0-1)$ emissions by the Argentine airglow spectrometer. Such cases provide an excellent opportunity to study the dynamics of the upper mesosphere with a higher than usual signal-to-noise ratio.

[3] The Meinel OH emission bands originate near 87 km altitude in the mesosphere and range from the visible spectrum to the infrared. They are the result of vibrational transitions in the ground state OH radical produced by the $H + O_3$ reaction [*Bates and Nicolet*, 1950]. The majority of the measured O($^1$S) 557.7 nm emission comes from the mesosphere near 96 km via the three-body *Barth* [1964] reaction. A small proportion, less than 20% [*Jacka*, 1984], originates from 250–300 km due to the dissociative recombination of $O_2^+$ ions in the *F* region [*Biondi and Feibelman*, 1968]. The near-infrared $O_2$ Atmospheric band emission at 861–870 nm is excited by the same three-body association reaction as the mesospheric 557.7 nm emission, and originates from near 95 km altitude. Not surprisingly, both emissions are strongly correlated.

[4] The El Leoncito Observatory location provides a unique opportunity for the investigation of dynamics at a midlatitude site in the southern hemisphere, a region relatively undersampled to date. It is located at 2500 m elevation, not far from the highest summits of the Andes, a known source of orographically generated gravity waves.

### 1.1. Mesospheric Wall Events and Bores

[5] As well as the ubiquitous QM gravity wave activity, there is a class of relatively uncommon mesospheric wave

[1]Center for Space Physics, Boston University, Boston, Massachusetts, USA.
[2]Instituto de Astronomía y Física del Espacio, Consejo de Investigaciones Científicas y Técnicas, Universidad de Buenos Aires, Buenos Aires, Argentina.


0148-0227/06/2005JA011197$09.00

phenomena which are characterized by a frontal onset of airglow brightness enhancement or depletion, followed by a series of propagating waves. Several frontal wave events have been reported in the literature, and they seem to fall into two distinct groups of events: (1) wall events [e.g., *Swenson and Espy*, 1995; *Swenson et al.*, 1998; *Batista et al.*, 2002] and (2) bore events [e.g., *Taylor et al.*, 1995b; *Smith et al.*, 2003; *Medeiros et al.*, 2005; *Fechine et al.*, 2005]. Each group is a distinctly different type of wave phenomenon, yet they exhibit similar morphologies in all-sky images and have similar lifetimes ranging from ~1 to several hours, so a careful interpretation is required to distinguish them.

[6] The prototype wall event occurred during the ALOHA-93 campaign [*Swenson and Espy*, 1995]. Subsequent analysis [*Swenson et al.*, 1998] indicated the event was a large upward propagating internal gravity wave that was in the process of breaking. Wall events typically exhibit a vertical phase variation between the wave patterns in the different airglow emissions ($O(^1S)$ and OH, for example), consistent with upward propagation.

[7] Internal mesospheric bores are nonlinear step-like disturbances which typically exhibit a series of trailing waves (sometimes called an undular bore). The first mesospheric bore candidate was reported by *Taylor et al.* [1995b], during the ALOHA-93 campaign, and there have been several subsequent reports of mesospheric bores [*Smith et al.*, 2003, 2005; *Brown et al.*, 2004; *She et al.*, 2004; *Medeiros et al.*, 2005; *Fechine et al.*, 2005; P. Loughmiller et al., Sharp mesospheric fronts: Dual bore theory and comparison to nonlinear numerical simulations, unpublished manuscript, 2006; P. Loughmiller et al., Sharp mesospheric fronts: Further observations of standard mesospheric bores and of new classes of bores, unpublished manuscripts, 2006]. The vertical phase difference of the resulting bore waves between airglow layers is typically either 0° or 180°. Although ducted gravity waves may exhibit this property, bores show additional distinguishing behaviors. The frontal character of a bore is very stable over time and causes either a sudden enhancement or depletion in the airglow emission (analogous to a DC offset), depending on the relative heights of the airglow layer and the disturbance. In the case of a ducted linear wave packet, the step-like disturbance (corresponding to a very wide spectrum of waves) would inevitably change shape due to dispersion. A bore disturbance may also have a propagating frontal onset without a series of trailing waves (sometimes called a turbulent bore). The individual wavefronts associated with an undular bore can propagate with different phase speeds (the leading wavefronts propagating faster than the trailing ones) and is a consequence of amplitude ordering (the works of *Mahapatra et al.* [1991] and *Smith et al.* [2003] are good examples). Furthermore, the number of trailing wavefronts associated with a bore may increase with time as the disturbance dissipates. Another very important aspect of internal bores is that they, unlike wall events, require a stable layer (or duct), such as a temperature inversion layer, in which to form and to propagate. Bores propagate horizontally and can travel large distances without significant attenuation. For example, *Smith et al.* [2003] reported that a naked-eye bore over Texas had propagated a horizontal distance of over 1200 km.

## 2. Observations and Analysis

[8] The Boston University all-sky imaging system [*Baumgardner et al.*, 1993] at Complejo Astronómico El Leoncito (CASLEO) has been operating since February 1999. The system utilizes a 384 × 256 pixel image-intensified charge-coupled device (ICCD) behind a rotating filter wheel which houses up to six narrow-band (1.2–1.8 nm FWHM) filters. The filters record several oxygen emissions from several height regimes: mesospheric $O(^1S)$ from near 96 km in altitude (557.7 nm), thermospheric $O(^1D)$ 630.0 nm emission from ~250 km, and $O(^5P)$ emission (777.4 nm) from above 300 km. A filter centered at 644.4 nm is used to monitor continuum emission and the two other positions are used for calibration purposes.

[9] The Argentine airglow spectrometer is a tilting interference filter design [*Scheer*, 1987; *Scheer and Reisin*, 2001] and has obtained mesospheric OH(6-2) zenith rotational temperature and brightness measurements at El Leoncito since 1984 (during short campaigns [e.g., *Scheer*, 1995]), and quasi-continuously since 1997 [e.g., *Scheer et al.*, 2005a]. Data were available during eleven hours for each of the two August nights (corresponding to 320 and 370 useable data points, respectively).

[10] The all-sky images were processed via our standard analysis routine: the images were corrected for vignetting by the optical system and for line-of-sight viewing effects, such as van Rhijn brightening near the horizon. The images were then corrected geometrically for distortion by the lens system (unwarped) and mapped to the assumed layer heights above the Earth's surface.

[11] The level of geomagnetic activity prior to the two events was relatively low. On 22 August, the 3-hour $K_p$ index in the prior 12 hours ranged from $1^+$ to $2^-$, and during the event, $2^0$. On the 23 August, the 3-hour $K_p$ index ranged from 0 to $2^+$, and during the event, $5^0$. Therefore it is reasonable to assume that the 557.7 nm $O(^1S)$ emission was predominately mesospheric in origin, i.e., no auroral or excessive thermospheric contaminations.

[12] On both nights, the two wave disturbances were also recorded very faintly in the 777.4 nm and 630.0 nm images. The 777.4 nm $O(^5P)$ emission is used typically to measure F2 layer structures over a broad height range centered near 350 km and arises from the radiative recombination of $O^+$ ions and electrons in the *F* region ionosphere. The 630.0 nm $O(^1D)$ emission originates from the 250–300 km height region and is due to the dissociative recombination of $O_2^+$ ions in the *F* region. We will show that the disturbance was a purely mesospheric event and that its visibility in the 777.4 nm and 630.0 nm images was due an enhancement of normally faint mesospheric OH emission lines located in the filters' transmission bandwidths. In the case of the 777.4 nm filter (FWHM = 1.6 nm), two OH spectral features: (1) $Q_1(3)$ doublet emission at 777.3 nm, and (2), $P_2(1)$ line emission at 778.4 nm, of the mesospheric OH(9-4) Meinel band, originate from near 87 km in altitude. There are also two emission lines: the $P_1(3)$ line at 630.68 nm and the $P_2(3)$ line at 629.80 nm from the mesospheric OH(9-3) band, with the potential for contamination of the 630.0 nm emission

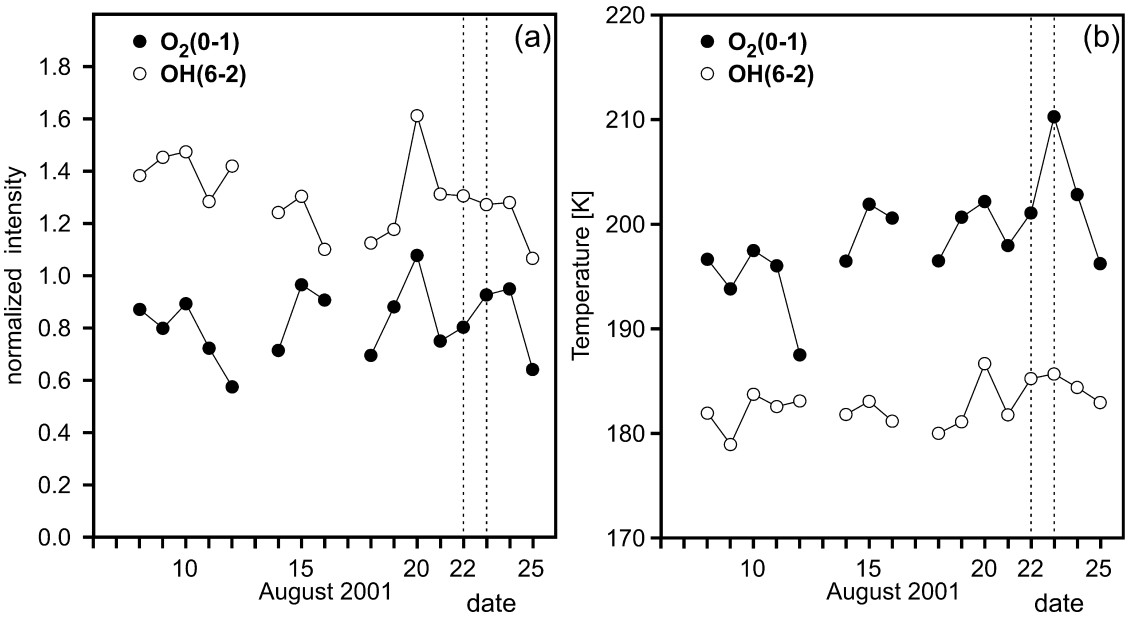


**Figure 1.** Nocturnal mean zenith (a) intensities and (b) rotational temperatures of the OH(6-2) and $O_2b(0-1)$ emission bands (normalized with respect to long-term means) observed by the Argentine airglow spectrometer during most of August 2001. The dates corresponding to the two nights under study are marked by the vertical dashed lines (dates start at 0000 UT). The statistical errors are generally less than the size of the symbols and, for the temperatures, are not greater than ±0.9 K for $O_2$ and ±0.6 K for OH.

(filter bandwidth FWHM = 1.2 nm) [*Hernandez*, 1974; *Burnside et al.*, 1977]. A similar type of enhancement of normally faint OH emission was observed in offband (644.4 nm) and 769.9 nm images during the naked-eye bore event reported by *Smith et al.* [2003].

[13] The 150–200 km height difference between the nighttime mesospheric 557.7 nm emission and the emissions recorded by the 630.0 nm and 777.4 nm filters, would be expected to result in significant differences in the observed spatial and temporal scales of the waves. However, the autocorrelation functions of the cross sections through the disturbance in the 557.7 nm, 777.4 nm and 630.0 nm images were, within the uncertainties, identical. Furthermore, the curvature and observed phase speed of the disturbance measured in the three emissions were similar. This suggests strongly that OH contamination was the reason for the appearance of the disturbance in the 777.4 and 630.0 nm images. As a result, the OH contamination in the 777.4 nm images provided valuable spatial and contextual information about the wave disturbances. We used the 777.4 nm images, because of the larger signal-to-noise ratio compared to the 630.0 nm images.

[14] Figure 1a shows the nocturnal mean intensities of the OH(6-2) and $O_2$ bands (normalized with respect to long-term means) observed by the airglow spectrometer, during most of August 2001. The $O_2$ and OH(6-2) intensities did not deviate much from the long-term average for the two nights. The normal seasonal level for $O_2$ (with respect to this average) is 0.75, and for OH, 1.0 and declining [*Scheer et al.*, 2005a]. The $O_2$ emission enhancement exhibited on the night of 20 August 2001 was accompanied by strong wave activity seen in the O($^1$S) images, in the $O_2$ intensities, but especially in the OH(6-2) intensities (several wave events during that night). This is consistent with the association between high airglow intensity and QM waves observed by *Scheer and Reisin* [2002; see also *Scheer et al.*, 2005b], the cause of which is still unknown.

[15] The nocturnal mean temperatures in the OH(6-2) layer (Figure 1b) were also comparable to the typical temperatures for that month. However, the $O_2$ layer showed a large increase of about 10 K for the night of 23 August with respect to its neighbors. Assuming that the airglow layer separation remained unchanged, the increase implies that the mean vertical temperature gradient was greater than in the other nights.

## 3. Wave Events

### 3.1. The 22 August 2001 Wave Event

[16] The bright mesospheric wave disturbance recorded on 22 August (see Figure 2) was first seen at 0645 UT and consisted of a set of small-scale, large-amplitude wavefronts propagating toward WNW (azimuth 285°E of north). The wavefronts were noticeably curved and extended across about two thirds of the sky. The entire event lasted ~3 hours and was also preceded by a similar but fainter event which lasted for ~0.5 hours between 0500 and 0530 UT. There was also some small wave activity propagating in a similar direction during the course of the night. Figure 2 also shows clearly that the signal-to-noise in the 777.4 nm images was much lower than in the 557.7 nm images.

[17] A series of ripples occurred along the two leading wavefronts of the disturbance. Ripples are small-scale (~1–5 km) wave-like structures, much smaller than gravity waves, that frequently occur in the nightglow emissions.

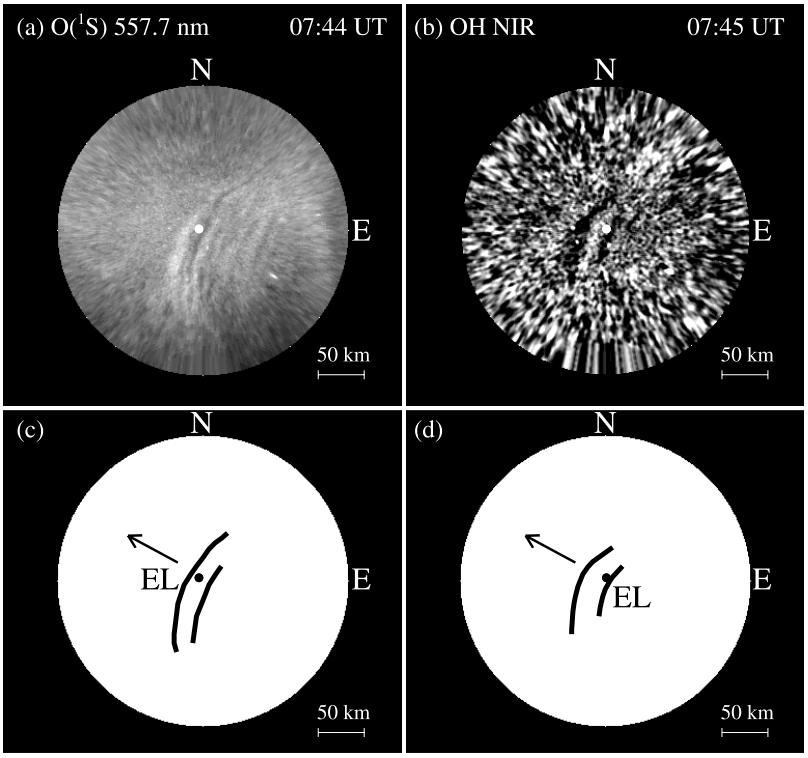


**Figure 2.** Two unwarped images in (a) 557.7 nm and (b) OH emission of the gravity wave disturbance on 22 August 2001 at El Leoncito. Tracings delineating the first two leading (c) light and (d) dark wavefronts in the 557.7 nm and OH emissions, respectively, are also shown. The disturbance exhibited markedly curved wavefronts and a surge-like behavior with complementary brightness patterns in the two emissions.

They do not propagate vertically and are believed to arise from instabilities within the local medium due to wind and wave activity [e.g., *Taylor and Hapgood*, 1990; *Hecht et al.*, 1997; *Yamada et al.*, 2001; *Hecht*, 2004]. The ripples were aligned perpendicular to the large waves and they disappeared at the end of the wave event, which suggested that the ripples were instabilities associated with the breaking or dissipation of the wave event. Their perpendicular orientation suggested that they were the result of convective instabilities, similar to those reported by *Hecht et al.* [1997], *Hecht* [2004], and *Li et al.* [2005a]. If they had been the result of dynamical instabilities, such as in the cases of *Taylor and Hapgood* [1990] or *Yamada et al.* [2001], one might expect them to be aligned perpendicular to the local wind flow and parallel to the wavefronts [see, e.g., *Taylor and Hapgood*, 1990; *Yamada et al.*, 2001; *Hecht et al.*, 2001, 2005; *Li et al.*, 2005b].

[18] Figure 3 shows two 557.7 nm and OH(777.4 nm) image cross sections through the 22 August event in the direction of wave propagation. The OH cross section has been horizontally shifted to take into account the time differences of the images and the phase speed of the disturbance. The cross sections have also been vertically shifted for clarity. The solid circles denote the positions of the bright and dark wavefronts in the O($^1$S) and OH emissions, and these show a clear difference in the scale size of the disturbance in the two emissions. The average horizontal wavelength was 20.4 ± 4.7 km in the O($^1$S) images, and 35.1 ± 5.0 km in the OH(777.4 nm) images.

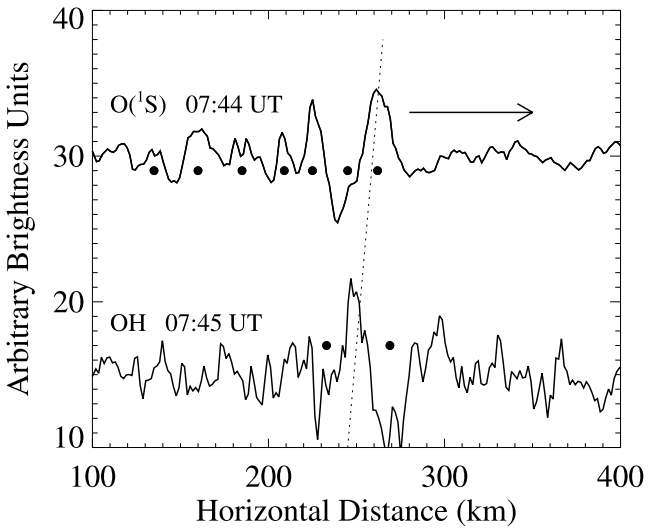


**Figure 3.** O($^1$S) and OH (777.4 nm) image cross sections (slices) of the 22 August wave event. The direction of propagation is shown by the arrow. The circles denote the positions of the O($^1$S)and OH wavefront positions. The OH slice has been shifted horizontally to account for the time difference between the two images. A line of constant phase (dashed) is drawn between two emissions, and the tilt indicates upward wave propagation.

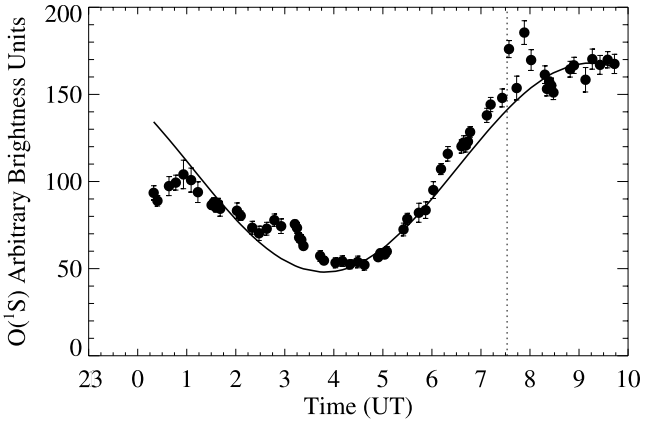


**Figure 4.** Time history of the 557.7 nm ($O(^1S)$) zenith brightness obtained from the all-sky images during the night of 22 August 2001. The brightness is dominated by a semidiurnal tidal variation with a period of 10.8 hours, as indicated by the least squares fit (solid curve). The two large jumps in the $O(^1S)$ brightness after 0730 UT (dashed vertical line) correspond to the zenith passage of the first two bright waves of the disturbance.

The average observed horizontal phase speed of the wavefronts, however, was very similar; $35 \pm 2$ ms$^{-1}$ in the $O(^1S)$ images and $34 \pm 4$ ms$^{-1}$ in the OH(777.4 nm) images, respectively, and remained constant in both emissions during the course of the event. The uncertainties in the speeds are the sample standard deviations and reflect geophysical as well as statistical variations in the measurements. The slope of the dashed line of constant phase is indicative of an upward propagating gravity wave. The difference in the two horizontal wavelengths in the two emissions indicates that the vertical wavelength increased with altitude.

[19] The brightness of all three airglow emissions was dominated by a large, long-period variation; the 557.7 nm $O(^1S)$ zenith emission brightness had a period of 10.8 hours, for example (see Figure 4), which was most probably associated with the semidiurnal tide. The wave disturbance can be seen as two positive large-amplitude oscillations (37% peak to peak compared to the mean brightness) just after 0730 UT. A slight decrease in the $O(^1S)$ emission brightness occurred for a short period of time after the passage of the disturbance. In comparison, Figure 5 shows the measured zenith airglow intensity (Figure 5a) and rotational temperature (Figure 5b) of the OH(6-2) and $O_2$ emissions obtained on the same night by the spectrometer. Both emissions are clearly dominated by a tidal variation similar to the $O(^1S)$ emission in Figure 4. The uncertainties in the individual OH(6-2) and $O_2$ temperature measurements have been plotted only for a few points (for clarity) but ranged from 2.8–6.5 K, and 2.5–10.3 K, respectively. The uncertainties in the individual intensity measurements ranged from 2.5–3.3% (the errors were deduced from photon counting statistics and error propagation through the conversion to rotational temperatures). In response to the wave disturbance, the OH(6-2) airglow brightness exhibited a rapid drop by 50% followed by another large-amplitude oscillation, just after 0730 UT, that lasted about 19 min. The $O_2$ brightness shows a strong wave train (consistent with Figure 2a), from 0740 UT until about 0900 UT, with a peak-to-peak amplitude of 21%. Typically, mesospheric gravity waves have amplitudes of 1–5% peak to peak. Only rarely are the peak-to-peak amplitudes observed to be greater than 15–20% (e.g., *Swenson and Espy* [1995] reported 30%, and *Sentman et al.* [2003] reported 15%). The OH intensity dips also coincided with the two jumps in the $O(^1S)$ emission brightness, and also with the dark bands visible in the OH(777.4 nm) image in Figure 2b, hence confirming that the 777.4 nm filter experienced

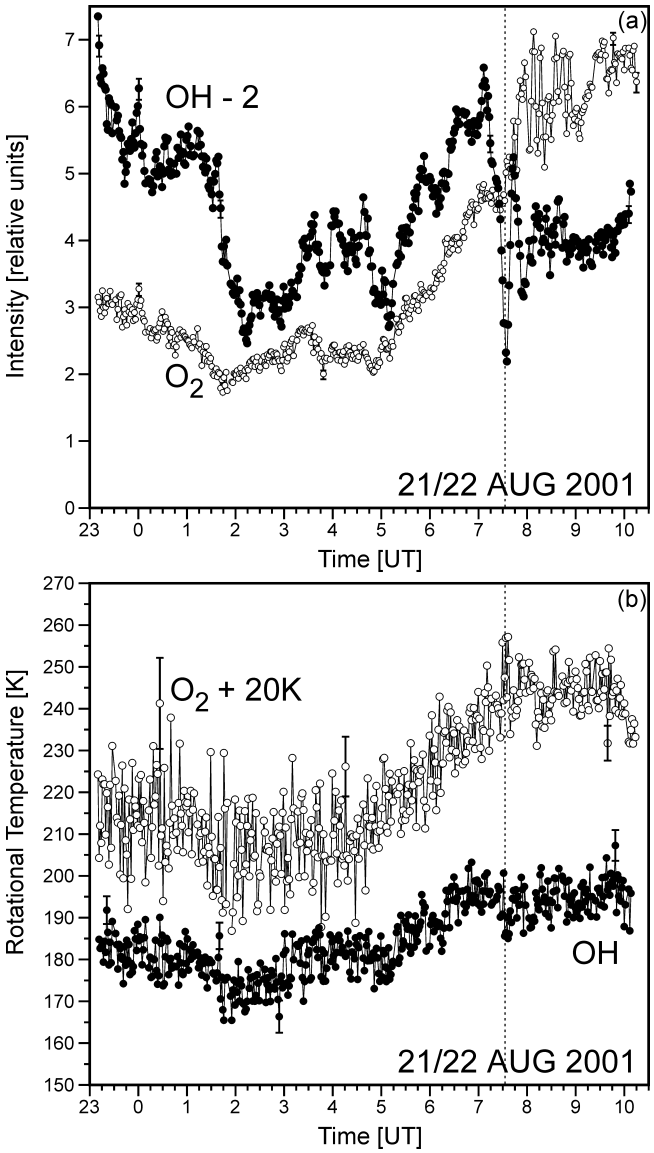


**Figure 5.** Time history of the OH and $O_2$ (a) zenith brightness and (b) temperatures obtained from spectrometer measurements on 22 August. The large intensity perturbation in the OH brightness due to the wave event is clearly evident near 0730 UT. For better legibility the OH intensities are shifted down by 2 relative units, and the $O_2$ temperatures are shifted up by 20 K. Error bars are shown only for some data points.

strong OH emission contamination. The disturbance also caused a drop of ~10 K in the OH(6-2) temperature.

[20] Figure 6 shows the data from Figures 4 and 5 but with the dominant tidal variation removed to emphasize the shorter timescale variations and the wave event in particular. Airglow brightness oscillations sample atmospheric waves at an equivalent altitude below the centroid height of the airglow layer, which leads to the observed phase shifts between airglow brightness and rotational temperature oscillations, if the waves propagate vertically [*Hines and Tarasick*, 1987; *Swenson and Gardner*, 1998]. So, in Figure 6, the intensity and temperature measurements from the different airglow layers have also been arranged vertically to reflect the different altitudes sampled by each parameter. The most striking feature is how different the disturbance was in the three emissions. The OH emission showed a large highly damped oscillation with a negative offset, whereas the $O_2$ emission showed the onset of a strong short-period wave packet. Furthermore, the O($^1$S) emission exhibited a similar, but antiphase, behavior to the OH emission. In all three emissions, the disturbance was superimposed asymmetrically on the slower variations.

[21] During the 0800–0900 UT interval, spectral analysis of the $O_2$ and OH(6-2) intensities obtained with the spectrometer yielded an observed period of $T_{obs}$ = 542 ± 2 s and $T_{obs}$ = 1200 ± 120 s, respectively. In comparison, the O($^1$S) and OH (777.4 nm) imaging measurements yielded observed wave periods of $T_{obs}$ = 582 ± 168 s and $T_{obs}$ = 1032 ± 270 s, respectively. The imaging O($^1$S) and the spectrometer $O_2$ values, in particular, agree very well, which is not surprising since they originate at similar altitudes (96 km & 95 km, respectively).

[22] We can treat the $O_2$ intensity wave as if it were a normal linear wave packet (in spite of its considerable amplitude). From the phase shift and amplitude ratio of the $O_2$ intensity and temperature oscillations, according to the *Hines and Tarasick* [1987] theory [see also *Reisin and Scheer*, 1996, 2001], the spectrometer measurements yielded a vertical wavelength of 45 ± 8 km. Using this value, and the horizontal wavelength obtained from the imager ($\lambda_x$ = 20.4 ± 4.7 km), the dispersion equation yields an intrinsic horizontal phase speed for the wave of $c_{int}$ = 63 ± 12 ms$^{-1}$ and an intrinsic period of $T_{int}$ = 319 ± 17 s. From the Doppler shift, we also deduced the horizontal wind component at 95–96 km in the direction of the wave to be −25 ± 4 ms$^{-1}$.

[23] The curvature of the wavefronts in Figure 2 suggests that the disturbance source was relatively small (~10–20 km) and located close, about 180 km, to the east of El Leoncito. The leading wavefront was first visible in the two emissions at a distance of ~50 km from the site, and the waves were upward propagating, so a possible origin for the disturbance could be a localized tropospheric or stratospheric disturbance. If the waves were launched from the tropopause region near 15 km altitude then, for an elevation angle for the group velocity vector of 66° (O($^1$S)) and 52° (OH) (= tan$^{-1}$ ($\lambda_z/\lambda_h$)), the waves would have traveled a horizontal distance of ~40 and 45 km, respectively, to reach the OH and O($^1$S) layers at 87 and 96 km, provided no refraction occurred during its journey. According to this argument, the wave source should have been no more than 90–95 km away, and not 180 km. The waves must therefore have experienced a sizable amount of refraction, or were Doppler-shifted (or both), during their journey into the upper atmosphere. A source region for the disturbance was sought but no clear precursor event could be determined. An analysis of GOES 8 satellite images indicated two long-lived convective regions; located ~650 km to the southeast and ~1000 km due east of El Leoncito but their positions were not consistent with the observed azimuth of the disturbance.

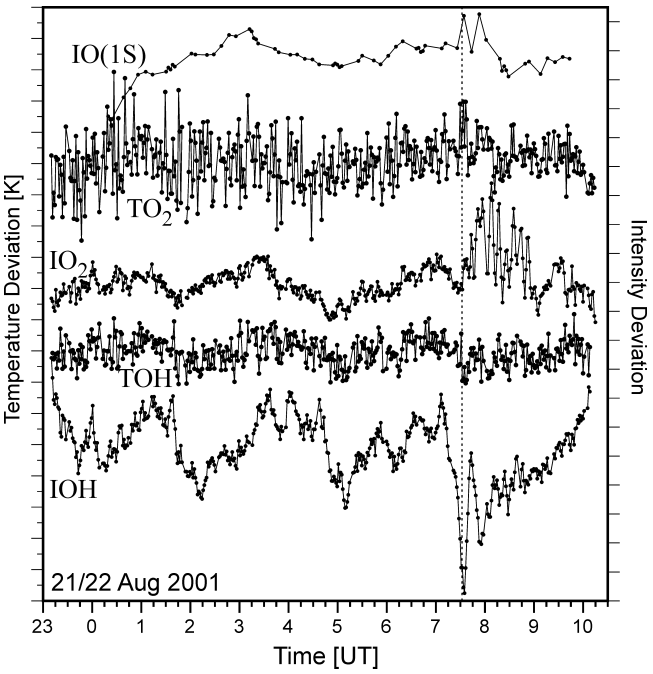


**Figure 6.** O($^1$S) intensity (all-sky imager) and OH and $O_2$ intensity (IOH, $IO_2$) and temperature (TOH, $TO_2$) measurements (airglow spectrometer) during the night of 22 August 2001. The dominant tidal features have been removed to emphasize the shorter timescale features. The time of the wave event is shown as the vertical dashed line. Each temperature tick mark corresponds to 10 K. The altitude variation of the disturbance is clearly evident.

[24] The vertical flux of the horizontal momentum ($F_M$) and energy ($F_E$) of the wave in the OH and $O_2$ emissions were estimated using the method of *Swenson and Liu* [1998] and *Liu and Swenson* [2003] with the caveat that the marked nonlinearity exhibited by the wave, particularly in the OH emission and less so in the $O_2$, probably lead to a larger error in the OH estimate than was obtained. The OH emission yielded values of $F_M$ = 408 ± 171 m$^2$ s$^{-2}$ and $F_E$ = 352 ± 210 mW m$^{-2}$, and the $O_2$ emission, $F_M$ = 128 ± 65 m$^2$ s$^{-2}$ and $F_E$ = 111 ± 76 mW m$^{-2}$. Moreover, the flux estimates for the 22 August event indicate that there was a significant amount of flux divergence over the nominal 8 km altitude, i.e., $\Delta F_M$ = 35 m$^2$ s$^{-2}$ km$^{-1}$ and $\Delta F_E$ = 30 mW m$^{-2}$ km$^{-1}$. The flux estimates are very large compared to typical average values obtained previously from all-sky measurements. *Swenson et al.* [1999], for example, reported momentum and energy flux values from gravity waves measured on five nights during February and April 1998 which averaged $F_M$ = 22 m$^2$ s$^{-2}$ ($\sigma$ = 9 m$^2$ s$^{-2}$) and $F_E$ =

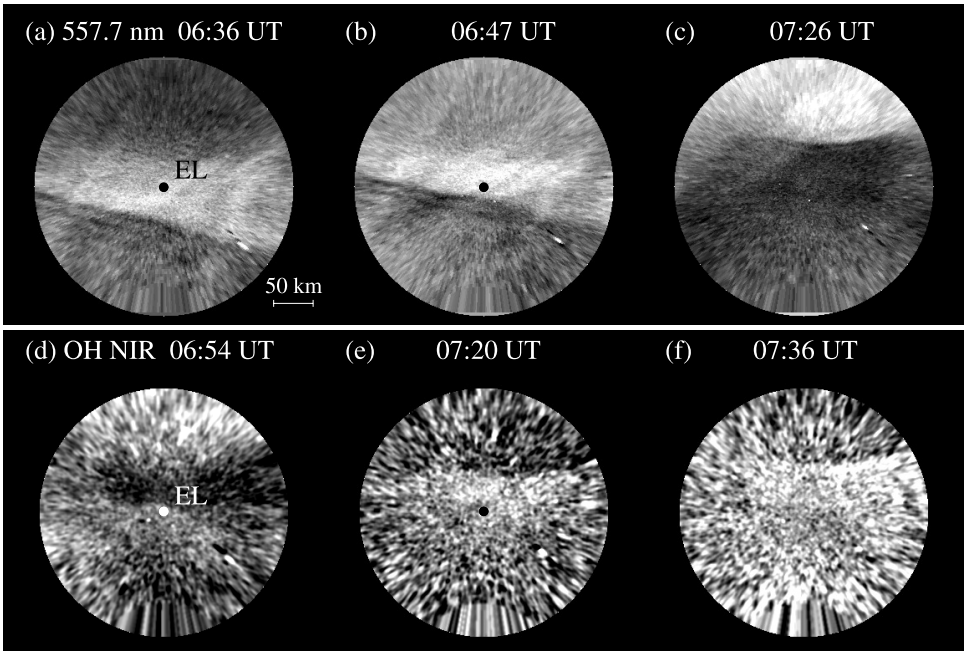


**Figure 7.** Sequence of unwarped images in (a–c) O($^1$S) 557.7 nm and (d–f) OH emission of the frontal wave disturbance on 23 August 2001 at El Leoncito. A train of waves follows the northward propagating front early on during the event (Figures 7a and 7b). In the OH images the front propagated due north, and no waves were detected. The complementary behavior in the emissions' brightness is clearly evident.

13 mW m$^{-2}$ ($\sigma$ = 4 mW m$^{-2}$)). However, gravity wave events with comparable momentum and energy flux values to the present event have been reported previously. Notably, the wall event reported by *Swenson and Espy* [1995], another large upward propagating gravity wave, which exhibited values of $F_M$ = 135 m$^2$ s$^{-2}$ and $F_E$ = 52 mW m$^{-2}$. More recently, *Sentman et al.* [2003] reported a gravity wave event in OH emission that was observed to originate from a thunderstorm complex. This event also exhibited similar momentum and energy flux values, $F_M$ = 144–253 m$^2$ s$^{-2}$ and $F_E$ = 83–97 mW m$^{-2}$.

### 3.2. The 23 August 2001 Wave Event

#### 3.2.1. Behavior and Identification

[25] The 23 August event was different from the previous night in several ways. In the O($^1$S) emission, an extensive, dark frontal disturbance propagated into a bright airglow background (see Figures 7a–7c). The front extended across the entire sky, at least 900 km at 96 km altitude, and was propagating toward 15° east of north. It was accompanied initially by a series of trailing waves. The waves were visible only on the western end of the disturbance (see Figures 7a and 7b). The eastern end exhibited only a dark trailing region. After the leading O($^1$S) front crossed the zenith, at about 0701 UT, the remaining trailing waves on the western end began to disappear and by 0715 UT, the entire frontal disturbance exhibited a dark trailing region with no waves. In addition, the propagation direction had rotated 15° counterclockwise to point due north. The leading frontal region had also become markedly curved with the concave side oriented toward the propagation direction (see Figure 7c). The curvature was opposite to that exhibited by the previous night's event. In the OH(777.4 nm) images, the disturbance showed a bright front propagating into a darker airglow region. No trailing waves were recorded in the OH(777.4 nm) images (Figures 7d–7f) because these images were obtained only after the trailing waves had already disappeared in the O($^1$S) images.

[26] Figure 8 shows the O($^1$S) zenith emission brightness measured by the all-sky imager during the course of the night. The brightness was dominated by a long-period (T ~ 10.1 hours) oscillation, which was probably associated with

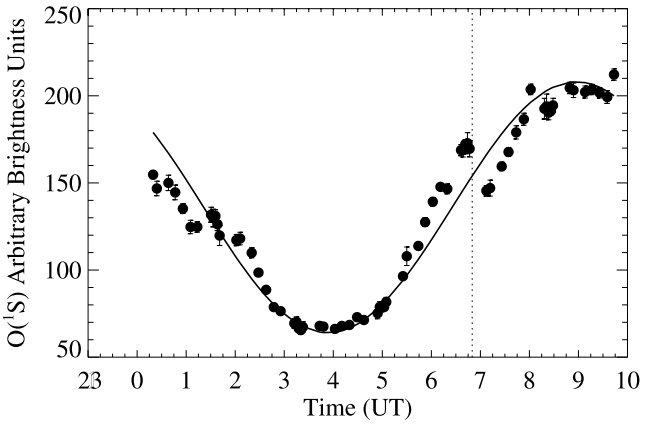


**Figure 8.** Time history of the 557.7 nm (O($^1$S)) zenith brightness obtained from the all-sky images during the night of 23 August 2001. The dashed vertical line denotes the zenith crossing time of the disturbance in the O($^1$S) emission. Similar to the previous night the brightness is dominated by a semidiurnal O($^1$S) tidal variation with a period of 10.1 hours, as indicated by the least squares fit (solid curve).

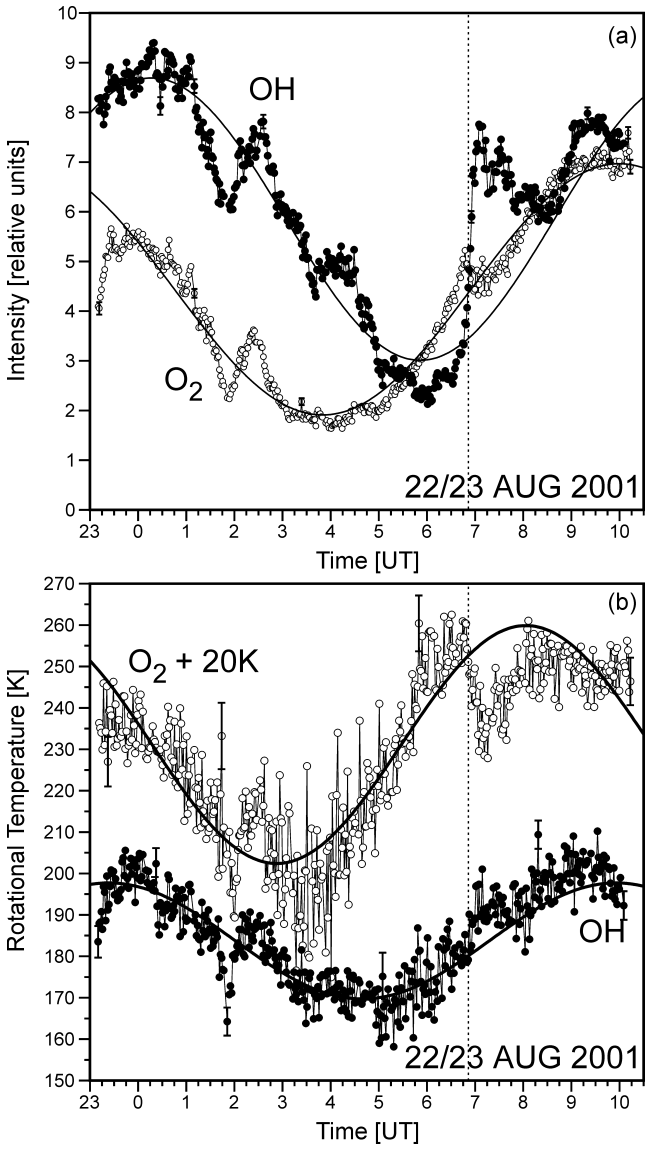


**Figure 9.** Time history of the OH and $O_2$ (a) zenith brightness and (b) temperatures obtained from spectrometer measurements on 23 August. The principal sinusoidal fits (with periods of about 12 hours) are also shown (see text). The wave event occurred at ~0700 UT and produced a large and sudden increase in OH brightness. The corresponding OH rotational temperatures showed a slower variation. As in Figure 5, the $O_2$ temperatures are shifted up by 20 K, and the error bars are signaled for some points.

the semidiurnal tide (see section 4). The disturbance occurred just before 7 UT (vertical dashed line), causing a sudden reduction in the O($^1$S) brightness. A small enhancement in the OH(777.4 nm) emission was also present (not shown). In comparison, in Figure 9, the OH(6-2) and $O_2$ intensity and temperature variations were also tidally dominated (Figure 9). Note also how the behavior of the $O_2$ intensity, and the temperature in particular, is very similar to that of the O($^1$S) brightness in Figure 8.

[27] Figure 10 shows the data from Figures 8 and 9, but with the dominant tidal variation removed to emphasize the shorter timescale variations. Similar to Figure 6, the parameters have also been arranged vertically to reflect the general height of occurrence of each parameter. The most striking feature is the large and sudden increase in the OH(6-2) emission brightness (by 2.5× in only about 15 min). Similarly to the 22 August event, the OH perturbation was superimposed asymmetrically on the large-scale intensity and brightness variations, which suggests the wave was nonlinear and not an ordinary linear gravity wave. The O($^1$S) and $O_2$ emissions exhibited similar sudden decreases in brightness, both opposite to the OH brightness behavior. The $O_2$ temperature decreased suddenly by 27 ± 2 K during the passage of the disturbance and the OH(6-2) temperature exhibited a short-lived temperature increase of 10 ± 2 K at the same time.

[28] Figure 11 shows cross sections made through two unwarped 557.7 nm and 777.4 nm images during the wave event in the direction of propagation. The frontal disturbance is clearly 180° out of phase in the two emissions, indicating some type of ducting is occurring. However, the sudden frontal increase in airglow brightness, the OH emission in particular, cannot be explained by a linear ducted gravity wave [*Munasinghe et al.*, 1998] and is more consistent with the behavior of a nonlinear type of disturbance such as an internal bore. Furthermore, the frontal disturbance continued to propagate across the sky well after the time that the trailing waves had disappeared. Such behavior is more consistent with a nonlinear type of

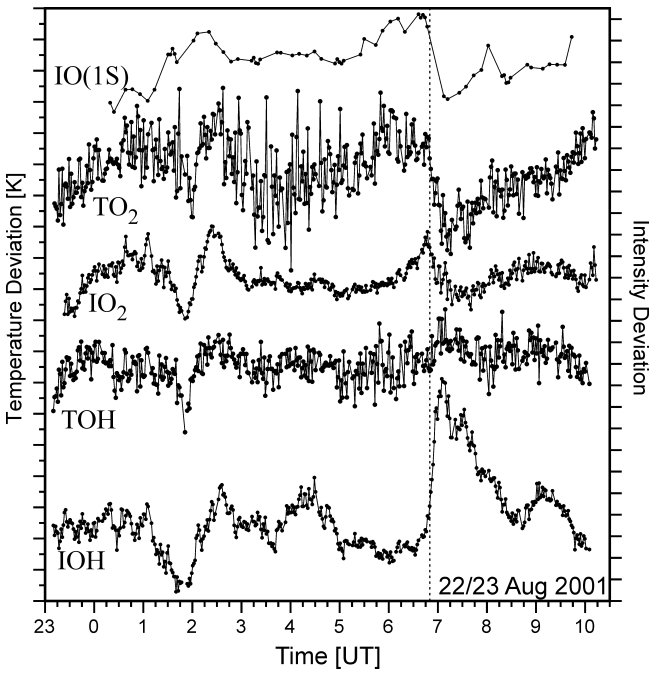


**Figure 10.** O($^1$S) intensity (all-sky imager) and OH and $O_2$ intensity (IOH, $IO_2$) and temperature (TOH, $TO_2$) measurements (airglow spectrometer) during the night of 23 August 2001. The dominant tidal features have been removed to emphasize the shorter timescale features. The time of the wave event is shown as the dashed vertical line. Each temperature tick mark corresponds to 10 K. The altitude variation of the disturbance is clearly evident, and the O($^1$S)/$O_2$ and OH intensity and temperature variations show a clear bipolar relationship.

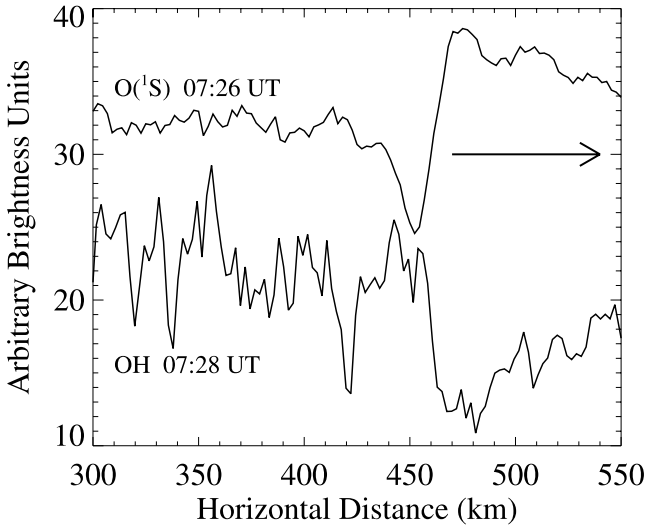


**Figure 11.** O($^1$S) and OH (777.4 nm) image cross sections (slices) made in the direction of propagation (arrow) of the 23 August wave event. The OH slice has been shifted horizontally to account for the propagation speed of the disturbance and the time difference between the two images. Despite the relatively large amount of noise present in the OH slice the relative phase shift of the front is clearly 180°.

disturbance in which the duct balances the amount of dispersion and wave growth, resulting in a stable sharp leading edge. This would not occur in a linear ducted gravity wave packet because a step-type disturbance consists of a wide spectrum of waves and the frontal jump would broaden over time due to dispersion.

[29] As described earlier, an internal bore is a horizontally propagating hydraulic jump or "step". Although bore disturbances are common in the oceans [e.g., *Osborne and Burch*, 1980; *Apel et al.*, 1985], rivers [e.g., *Tricker*, 1965; *Lighthill*, 1978], and in the lower atmosphere [e.g., *Smith*, 1988; *Mahapatra et al.*, 1991] they have only recently been identified in the mesosphere [*Taylor et al.*, 1995b; *Dewan and Picard*, 1998; *Smith et al.*, 2003; *She et al.*, 2004]. Mesospheric bores exhibit an extensive frontal onset which is accompanied by a series of trailing waves, and so is sometimes called an undular bore. Bores require a stable region in which to form and propagate, such as a temperature inversion or a wind shear, both of which occur frequently in the mesosphere.

[30] The temperature measurements suggested the presence of a large thermal inversion layer (a necessary condition for bore propagation) in the 85–95 km height region during the time of the disturbance. Figure 9b indicates that a gradient of +28 K over a nominal altitude of 8 km was present during the event. During August (southern summer), one would expect the mesopause (temperature minimum) to lie near or above 95 km, so an inversion was probably present, above the height of the OH layer, during the time of the event. The temperature gradient accounts for a bias in the $O_2$ layer temperature measurements of 22.3 ± 4.7 K [*Scheer et al.*, 2006].

### 3.2.2. Propagation Speed

[31] The positions of the first two bright (open circles) and dark (filled circles) wavefronts in the O($^1$S) images are shown in Figure 12a, together with second-order polynomial fits. The bore disturbance underwent a constant deceleration of 0.006 m s$^{-2}$ (21 m s$^{-1}$ hr$^{-1}$) during its lifetime, with an observed horizontal phase speed decreasing from 98 ± 5 m s$^{-1}$ to 61 ± 5 m s$^{-1}$. At zenith, the disturbance exhibited an observed horizontal phase speed of 75 ± 5 m s$^{-1}$. The eastern end of the disturbance also propagated slightly faster (by ~2 m s$^{-1}$) than the western end, resulting in a skewing of the front as it crossed the sky. This is the first time that a bore disturbance has been reported to decelerate during its passage across the sky. The deceleration was probably due to energy dissipation by the bore or to a change in the local wind speed, although no wind measurements were available at the site to verify this. Interestingly, the disturbance in the OH images propagated at a constant velocity of 61 ± 13 m s$^{-1}$, with no deceleration evident (Figure 12a).

[32] The horizontal wavelength ($\lambda_h$) in the O($^1$S) images decreased over time (see Figure 12b), a consequence of the deceleration of the disturbance. Between 0630 and 0700 UT, $\overline{\lambda_h}$ was 31.9 km ($\sigma$ = 5.2 km) with an observed period of 7.2 min. The dispersion equation yielded an estimate of the local wind, at 96 km altitude, of 25 m s$^{-1}$

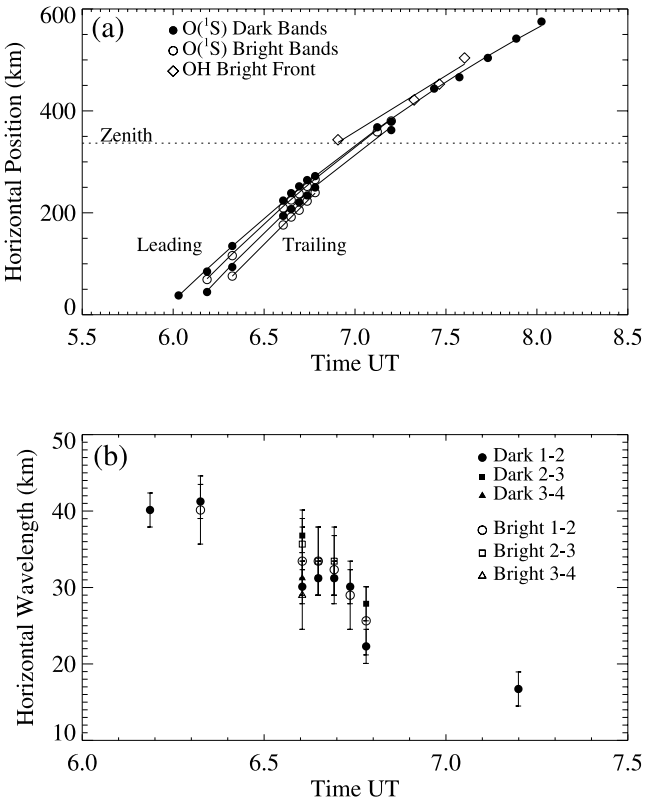


**Figure 12.** (a) Time history of the wavefront positions in the 23 August disturbance. The circles are associated with the O($^1$S) emission (dark wavefronts are solid; bright wavefronts are open), and the diamonds are associated with the OH emission. The uncertainties are smaller than the plot symbols. (b) Horizontal wavelengths associated with the 23 August disturbance. The solid symbols denote the dark wavefronts, and the open symbols denote the bright wavefronts.

**Table 1.** Least Squares Tidal Intensity and Temperature Amplitude Fits for the Nights of 22–23 August 2001

| | $\frac{I'}{I(OH)}$ | T(OH) | $\frac{I'}{I(O_2)}$ | $T(O_2)$ |
|---|---|---|---|---|
| 22 August | 0.18 | 10.6 K | 0.54 | 18.7 K |
| 23 August | 0.49 | 14.0 K | 0.57 | 28.7 K |

opposite to the direction of the disturbance. This result, in turn, leads to an intrinsic period of 5.4 min, which is very close to the Brunt-Väisälä period in the region and a strong indicator of wave resonance. Using the model equations (6)–(9) and (12) from *Dewan and Picard* [1998] and $\overline{\lambda_h}$, we estimate the depth of the ducting region to be 9.0 km, which is fairly typical of what has been reported previously.

## 4. Evidence for Tidal Control of Bore Occurrence

[33] Table 1 lists the least squares estimates of semidiurnal tidal amplitude during the nights of 22 and 23 August. The tidal variations were analyzed by removing the perturbations due to each night's wave event. Although this led to data gaps of <2–3 hours, the spectral analysis based on least squares fitting is capable of dealing adequately with the gaps. The uncertainties associated with the tidal parameters were 3% and were the result of several factors including: period uncertainty due to residual variance, comparison of the intensity and temperature periods, and error propagation. On both nights, the amplitude of the semidiurnal temperature oscillation (see Table 1) increased by a factor of two over a vertical height of about 8 km (from the OH to the $O_2$ layer, at 87 and 95 km, respectively), which indicated that there was little or no dissipation of the tidal oscillation. In particular, on 23 August, the night of the bore event, the tidal amplitude was among the greatest that has been observed at El Leoncito [*Reisin and Scheer*, 1996; *Scheer and Reisin*, 1990, 1998, 2002]: 58 K peak to peak at the $O_2$ layer. The vertical wavelength of the tidal oscillation on that night was estimated to be $\lambda_z = 33$ km at the OH level, and $\lambda_z = 48$ km at $O_2$. These estimates, again made via the *Hines and Tarasick* [1987] theory, are also consistent with an emission layer separation of 8 km [see *Reisin and Scheer*, 1996].

[34] The vertical temperature gradient between the OH and $O_2$ layers, due to the semidiurnal tide, was a maximum at 0714 UT (see Figure 9b), around the time of the disturbance. Furthermore, assuming the emission heights remained constant, the vertical temperature gradient during the night varied by 51 K. In contrast, during the previous night (22 August) the vertical gradient varied by only 17 K (with the minimum gradient occurring at 0235 UT, and the maximum after 1008 UT). On the 23 August, the fact that the onset time of the bore disturbance coincided with the maximum in the tidally induced vertical temperature gradient, combined with the increased semidiurnal tidal amplitude, suggests strongly that the occurrence of this particular bore was controlled by the semidiurnal tide.

## 5. Discussion

[35] The two wave events, unlike typical gravity waves, both exhibited large asymmetric perturbations with large amplitudes. For example, during the August 22 event, the OH and $O_2$ intensities showed markedly different responses to the perturbation (see Figure 6). A heavily damped oscillation with a clear negative offset was seen in the OH emission, whereas the $O_2$ emission showed a very clear and long-lived oscillation with a positive offset (it was also the longest monochromatic wave train ever observed in over 1300 nights at El Leoncito).

[36] The model developed by *Liu and Swenson* [2003], which investigates the effect of gravity waves in the OH and $O_2$ emissions, was used in our analysis and interpretation. The strong nonlinear behavior of the events, however, severely limits the usefulness of the model, which assumes linear perturbations. It did show, however, that the 22 August event was consistent with a large-wavelength, upward propagating gravity wave, with a vertical wavelength of 45 km, as determined by the imaging and spectrometric measurements. The damped, asymmetric perturbation seen in the OH emission on both nights is also very similar to the results of a nonlinear internal mesospheric bore model developed by *Seyler* [2005]; in particular, Figures 5 and 6 of that study. Another interesting aspect of the 22 August event was that the times of the perturbation maxima and minima in the OH emission were not equally spaced, as expected in a linear wave, but increased away from the leading edge of the disturbance (see Table 2). This behavior suggests that wave was experiencing some degree of nonlinearity due to breaking or saturation.

[37] From these measurements, we conclude that although the event as observed at 96 km was a large upward propagating gravity wave, with a wavefront curvature even at the OH level, consistently pointing toward a not very distant source, the amplitude and waveshape at 87 km seem to be inconsistent with a simple linear wave interpretation. The event did not show the extensive frontal onset which is characteristic of a wall event [e.g., *Swenson and Espy*, 1995]. The apparent proximity of the source to El Leoncito could be one reason for this.

[38] The 23 August event, on the other hand, was different in several respects. An extensive propagating frontal boundary separating a large-scale decrease in the $O(^1S)$ airglow brightness and $O_2$ temperature, and, in particular, a very strong increase in OH brightness, as the disturbance propagated over the site. The trailing waves associated with the front were also in antiphase in the $O(^1S)$ and OH emissions.

[39] We investigated the possibility that the extensive and sudden change in airglow intensity was the result of a large-scale region of enhanced atomic oxygen moving over the observing site, due to downward advection from 100 km by a transient gravity wave packet. This would be expected to cause an increase in OH brightness without any significant increase in OH temperature and $O_2$ brightness. However, Figure 10 indicates that the OH layer temperature did increase by 10 ± 2 K as a result of the disturbance, and

**Table 2.** Time Differences Between OH Maxima and Minima During the 22 August 2001 Wave Event

| Feature | Time Difference |
|---|---|
| First minimum to second maximum | $8^m13^s$ |
| Second maximum to second minimum | $10^m52^s$ |
| Second minimum to third maximum | $16^m44^s$ |

the $O_2$ and O($^1$S) emissions both showed strong brightness decreases. The $O_2$ emission also showed a corresponding temperature decrease of 27 ± 2 K. Therefore we do not believe the event was related to advection.

[40] The stability of the sharp frontal boundary over the course of the event (see Figures 7a–7c) suggested that the disturbance was nonlinear in nature. In the case of a ducted linear wave packet, the sharp front (corresponding to a very wide spectrum of waves) would inevitably change shape due to dispersion. In a nonlinear bore case, the effects of dispersion and wave growth are in stable balance [*Lighthill*, 1978]. The front continued to propagate across the sky even after the set of trailing waves, seen in the O($^1$S) images (Figures 7a–7c), had disappeared leaving the trailing region of depleted O($^1$S) emission. The region was probably then turbulent, analogous to the behavior of nonundular river bores which exhibit a trailing region of turbulence on occasion.

[41] The large-scale morphology of the disturbance in all three emissions (the OH emission in particular) was strongly asymmetric. The large-scale intensity and temperature variations, i.e., the envelope, of the 23 August wave event are consistent with a ducted wave packet that was propagating above the OH layer and below the O($^1$S) and $O_2$ layers, i.e., centered between 88 and 93 km. It displaced these two airglow layers downward and upward, respectively, causing the inversely correlated OH and O($^1$S)/$O_2$ brightness and temperature variations. The disturbance caused a marked increase in OH brightness, and temperature by 10 ± 2 K, and a simultaneous decrease in the brightness of the O($^1$S) and $O_2$ emissions. The $O_2$ temperature also decreased by 27 ± 2 K. Using the temperature values, we estimate the ducting depth changed by −1 km at 87 km (OH) and by +2.7 km at 95 km (O($^1$S)). This behavior is consistent with a varicose mode internal bore [*Dewan and Picard*, 1998; *Seyler*, 2005], a nonlinear ducted wave disturbance, propagating within a ducting region centered above the OH layer but below the $O_2$ and O($^1$S) layers. The modeling results by *Seyler* [2005] suggest that an ordinary ducted wave can develop frequently nonlinear behavior similar to a bore disturbance; a duct being a necessary condition for bore production, as well as for propagation.

[42] We compared the morphology of the 23 August event to the eight bore identification criteria given by *Dewan and Picard* [2001]. The morphology and behavior of the 23 August wave was consistent with most of the criteria but, except for the sharp frontal feature, did not differ substantially from an ordinary ducted wave packet. For example, the disturbance had initially an observed horizontal phase speed which was consistent with both a bore and an ordinary ducted wave. The number of trailing waves associated with a bore usually increases over time, as the disturbance dissipates energy. In the case of the 23 August event, it appeared that the bore disturbance was dissipating as a whole and that the trailing waves were disappearing, so no evidence was found for an increase in the number of waves during the disturbance.

[43] Although no wind measurements were available at El Leoncito, the observed temperature tide suggests that as the tidal winds varied over the course of the night, the disturbance was allowed to propagate up into the airglow layers. Similarly, during the large bore event over Texas [*Smith et al.*, 2003], mesospheric wind measurements from a meteor radar indicated that a large vertical wind shear occurred in the 85–95 km height region, just prior to appearance of the bore.

## 6. Conclusion

[44] The two events presented here demonstrate some of the diversity of dynamical phenomena in the mesopause region at El Leoncito. They also illustrate the importance of multidiagnostic measurements in the interpretation and characterization of wave phenomena in the region. The mesospheric effort at El Leoncito will soon be enhanced greatly with the addition of a suite of new diagnostic systems. These systems will provide simultaneous imaging, wind, and temperature measurements of the wave propagation environment in the mesosphere at a Southern hemisphere site. In addition to the airglow instruments used here, we soon hope to have data from a VHF all-sky Interferometric Meteor Radar system (SKiYMET) at El Leoncito. The system will provide horizontal wind profile measurements from the 80–110 km height region [*Mitchell et al.*, 1999; *Pancheva et al.*, 2004] and will allow intrinsic gravity wave parameters to be determined. A new Boston University bare CCD all-sky imager will provide measurements with enhanced sensitivity.

[45] **Acknowledgments.** The authors would like to thank the director and staff at CASLEO for their continued support for our observation program at El Leoncito. We gratefully acknowledge that this study was supported by the NSF CEDAR program under grant ATM 0123064, the NSF Aeronomy Program under grant ATM 0322875, and the Office of Naval Research under grant N00014-03-1-0069. We are also grateful to J. L. Minetti of the University of Tucumán, Argentina, for providing us with meteorological data. J.S. and E.R.R. acknowledge partial funding by CONICET and ANPCyT grants PIP 4554/96 and PICT 12187.

[46] Arthur Richmond thanks Gary Swenson and another reviewer for their assistance in evaluating this paper.

## References

Apel, J. R., J. R. Holbrook, A. K. Liu, and J. J. Tsai (1985), The Sulu Sea internal experiment, *J. Oceanogr.*, *15*, 1625–1651.

Barth, C. A. (1964), Three body reactions, *Ann. Geophys.*, *20*, 182–196.

Bates, D. R., and M. Nicolet (1950), The photochemistry of atmospheric water vapor, *J. Geophys. Res.*, *55*, 301–327.

Batista, P. P., B. R. Clemesha, D. M. Simonich, M. J. Taylor, H. Takahashi, D. Gobbi, I. S. Batista, R. A. Buriti, and A. F. Medeiros (2002), Simultaneous lidar observation of a sporadic sodium layer, a "wall" event in the OH and OI 5577 airglow images and the meteor winds, *J. Atmos. Sol. Terr. Phys.*, *64*, 1327–1335.

Baumgardner, J., B. Flynn, and M. Mendillo (1993), Monochromatic imaging instrumentation for applications in aeronomy of the earth and planets, *Opt. Eng.*, *32*(12), 3028–3032.

Biondi, M. A., and W. A. Feibelman (1968), Twilight and nightglow emission spectral line shapes of oxygen λ6300 and λ5577 radiation, *Planet. Space Sci.*, *16*, 431–443.

Brown, L. B., A. J. Gerrard, J. W. Meriwether, and J. J. Makela (2004), All-sky imaging observations of mesospheric fronts in OI 557. 7 nm and broadband OH emissions: Analysis of frontal structure, atmospheric background conditions, and potential sourcing mechanisms, *J. Geophys. Res.*, *109*, D19104, doi:10.1029/2003JD004223.

Burnside, R. G., J. W. Meriwether, and M. R. Torr (1977), Contamination of ground-based measurements of OI (6300 Å) and NI (5200 Å) airglow by OH emissions, *Planet. Space. Sci.*, *25*(10), 985–988.

Dewan, E. M., and R. H. Picard (1998), Mesospheric bores, *J. Geophys. Res.*, *103*, 6295–6305.

Dewan, E. M., and R. H. Picard (2001), On the origin of mesospheric bores, *J. Geophys. Res.*, *106*, 2921–2927.

Fechine, J., A. F. Medeiros, R. A. Buriti, H. Takahashi, and D. Gobbi (2005), Mesospheric bore events in the equatorial middle atmosphere, *J. Atmos. Sol. Terr. Phys.*, *67*(17–18), 1774–1778.

Hecht, J. H. (2004), Instability layers and airglow imaging, *Rev. Geophys.*, *42*, RG1001, doi:10.1029/2003RG000131.

Hecht, J. H., R. L. Walterscheid, D. C. Fritts, J. R. Isler, D. C. Senft, C. S. Gardner, and S. J. Franke (1997), Wave breaking signatures in OH airglow and sodium densities and temperatures 1. Airglow imaging, Na lidar, and MF radar observations, *J. Geophys. Res.*, *102*, 6655–6668.

Hecht, J. H., R. L. Walterscheid, and R. A. Vincent (2001), Airglow observations of dynamical (wind shear-induced) instabilities over Adelaide, Australia associated with atmospheric gravity waves, *J. Geophys. Res.*, *106*, 28,189–28,197.

Hecht, J. H., A. Z. Liu, R. L. Walterscheid, and R. J. Rudy (2005), Maui Mesosphere and Lower Thermosphere (Maui MALT) observations of the evolution of Kelvin-Helmholtz billows formed near 86 km altitude, *J. Geophys. Res.*, *110*, D09S10, doi:10.1029/2003JD003908.

Hernandez, G. (1974), Contamination of the OI ($^3P_2$-$^1D_2$) emission line by the (9–3) band of OH $X^2\Pi$ in high-resolution measurements of the night sky, *J. Geophys. Res.*, *79*, 1119–1123.

Hines, C. O., and D. W. Tarasick (1987), On the detection and utilization of gravity waves in airglow studies, *Planet. Space Sci.*, *35*, 851–866.

Jacka, F. (1984), Application of Fabry-Perot spectrometers for measurement of upper atmosphere temperatures and winds, in *Handbook for Middle Atmosphere Program*, vol. 13, edited by R. A. Vincent, pp. 19–40, SCOSTEP Secr., Univ. of Ill., Urbana-Champaign.

Li, F., A. Z. Liu, G. R. Swenson, J. H. Hecht, and W. A. Robinson (2005a), Observations of gravity wave breakdown into ripples associated with dynamical instabilities, *J. Geophys. Res.*, *110*, D09S11, doi:10.1029/2004JD004849.

Li, T., C. Y. She, B. P. Williams, T. Yuan, R. L. Collins, L. M. Kieffaber, and A. W. Peterson (2005b), Concurrent OH imager and sodium temperature/wind lidar observation of localized ripples over northern Colorado, *J. Geophys. Res.*, *110*, D13110, doi:10.1029/2004JD004885.

Lighthill, M. J. (1978), *Waves in Fluids*, 504 pp, Cambridge Univ. Press, New York.

Liu, A. Z., and G. R. Swenson (2003), A modeling study of $O_2$ and OH airglow perturbations induced by atmospheric gravity waves, *J. Geophys. Res.*, *108*(D4), 4151, doi:10.1029/2002JD002474.

Mahapatra, P. R., R. J. Doviak, and D. S. Zrnic (1991), Multisensor observation of an atmospheric undular bore, *Bull. Am. Meteorol. Soc.*, *72*, 1468–1480.

Medeiros, A. F., J. Fechine, R. A. Buriti, H. Takahashi, C. M. Wrasse, and D. Gobbi (2005), Response of OH, $O_2$ and OI5577 airglow emissions to the mesospheric bore in the equatorial region of Brazil, *Adv. Space Phys.*, *35*(11), 1971–1975.

Mitchell, N., H. R. Middleton, A. G. Beard, P. J. S. Williams, and H. G. Muller (1999), The 16–day planetary wave in the mesosphere and lower thermosphere, *Ann. Geophys.*, *17*, 1447–1456.

Munasinghe, G., H. Hur, T. Y. Huang, A. Battachryya, and T. F. Tuan (1998), Application of the dispersion formula to long- and short-period gravity waves: Comparisons with ALOHA-93 data and an analytical model, *103*, 6467–6481.

Osborne, A. R., and T. L. Burch (1980), Internal solitons in the Andaman Sea, *Science*, *208*, 451–460.

Pancheva, D., N. Mitchell, and P. Younger (2004), Meteor radar observations of atmospheric waves in the equatorial mesosphere/lower thermosphere over Ascension Island, *Ann. Geophys.*, *22*, 387–404.

Reisin, E. R., and J. Scheer (1996), Characteristics of atmospheric waves in the tidal period range derived from zenith observations of $O_2$(0–1) atmospheric and OH (6–2) airglow at lower midlatitudes, *J. Geophys. Res.*, *101*, 21,223–21,232.

Reisin, E. R., and J. Scheer (2001), Vertical propagation of gravity waves determined from zenith observations of airglow, *Adv. Space Res.*, *27*(10), 1743–1748.

Scheer, J. (1987), Programmable tilting filter spectrometer for studying gravity waves in the upper atmosphere, *Appl. Opt.*, *26*, 3077–3082.

Scheer, J. (1995), What can be learned from rotational temperatures derived from ground-based airglow observations about the aeronomy of the Southern Hemisphere, *Adv. Space Res.*, *16*(5), 61–69.

Scheer, J., and E. R. Reisin (1990), Rotational temperatures for OH and $O_2$ airglow bands measured simultaneously from El Leoncito (31°48′S), *J. Atmos. Terr. Phys.*, *52*, 47–57.

Scheer, J., and E. R. Reisin (1998), Extreme intensity variations of $O_2b$ airglow induced by tidal oscillations, *Adv. Space Res.*, *21*(6), 827–830.

Scheer, J., and E. R. Reisin (2001), Refinements of a classical technique of airglow spectroscopy, *Adv. Space Res.*, *27*(6–7), 1153–1158.

Scheer, J., and E. R. Reisin (2002), Most prominent airglow night at El Leoncito, *J. Atmos. Sol. Terr. Phys.*, *64*, 1175–1181.

Scheer, J., E. R. Reisin, and C. H. Mandrini (2005a), Solar activity signatures in mesopause region temperatures and atomic oxygen related airglow brightness at El Leoncito, Argentina, *J. Atmos. Sol. Terr. Phys.*, *67*(1–2), 145–154, doi:10.1016/j.jastp.2004.07.023.

Scheer, J., E. R. Reisin, P. P. Batista, B. R. Clemesha, and H. Takahashi (2005b), Detection of meteor radar wind signatures related to strong short-duration day-to-day airglow transitions at sites 2600 km apart, *J. Atmos. Sol. Terr. Phys.*, *67*(6), 611–621, doi:10.1016/j.jastp.2004.12.007.

Scheer, J., E. R. Reisin, O. A. Gusev, W. J. R. French, G. Hernandez, R. Huppi, P. Ammosov, G. A. Gavrilyeva, and D. Offermann (2006), Use of CRISTA mesopause region temperatures for the intercalibration of ground-based instruments, *J. Atmos. Sol. Terr. Phys*, doi:10.1016/j.jastp.2005.12.009, in press.

Sentman, D. D., et al. (2003), Simultaneous observations of mesospheric gravity waves and sprites generated by a Midwestern thunderstorm, *J. Atmos. Sol. Terr. Phys.*, *65*, 537–550.

Seyler, C. E. (2005), Internal waves and undular bores in mesospheric inversion layers, *J. Geophys. Res.*, *110*, D09S05, doi:10.1029/2004JD004685.

She, C. Y., T. Li, B. P. Williams, Tao Yuan, and R. H. Picard (2004), Concurrent OH imager and sodium temperature/wind lidar observations of a mesopause undular bore event over Fort Collins/Platteville, CO, *J. Geophys. Res.*, *109*, D22107, doi:10.1029/2004JD004742.

Smith, R. K. (1988), Traveling waves and bores in the lower atmosphere: The 'Morning Glory' and related phenomena, *Earth Sci. Rev.*, *25*, 267–290.

Smith, S. M., M. Mendillo, J. Baumgardner, and R. R. Clarke (2000), Gravity wave imaging from a sub-auroral site: First results from Millstone Hill, *J. Geophys. Res.*, *105*, 27,119–27,130.

Smith, S. M., M. J. Taylor, G. R. Swenson, C. Y. She, W. Hocking, J. Baumgardner, and M. Mendillo (2003), A multidiagnostic investigation of the mesospheric bore phenomenon, *J. Geophys. Res.*, *108*(A2), 1083, doi:10.1029/2002JA009500.

Smith, S. M., J. Friedman, S. Rashida, C. Tepley, J. Baumgardner, and M. Mendillo (2005), Evidence of mesospheric bore formation from a breaking gravity wave event: Simultaneous imaging and lidar measurements, *J. Atmos. Sol. Terr. Phys.*, *67*, 345–356, doi:10.1016/j.jastp.2004.11.008.

Swenson, G. R., and P. J. Espy (1995), Observations of 2–dimensional airglow structure and Na density from the ALOHA, October 9, 1993 'storm flight', *Geophys. Res. Lett.*, *22*, 2845–2848.

Swenson, G. R., and C. S. Gardner (1998), Analytical models for the responses of the mesospheric OH* and Na layers to atmospheric gravity waves, *J. Geophys. Res.*, *103*, 6271–6294.

Swenson, G. R., and A. Z. Liu (1998), A model for calculating acoustic gravity wave momentum flux in the mesosphere from OH airglow, *Geophys. Res. Lett.*, *25*, 477–480.

Swenson, G. R., J. Qian, J. M. C. Plane, P. J. Espy, M. J. Taylor, D. N. Turnbull, and R. P. Lowe (1998), Dynamical and chemical aspects of the mesospheric Na "wall" event on October 9, 1993 during the Airborne Lidar and Observations of Hawaiian Airglow (ALOHA) campaign, *J. Geophys. Res.*, *103*, 6361–6380.

Swenson, G. R., R. Haque, W. Yang, and C. S. Gardner (1999), Momentum and energy fluxes of monochromatic gravity waves observed by an OH imager at Starfire Optical Range, New Mexico, *J. Geophys. Res.*, *104*, 6067–6080.

Taylor, M. J., and M. A. Hapgood (1990), On the origin of ripple-type structure in the OH nightglow emission, *Planet. Space Sci.*, *38*, 1421–1430.

Taylor, M. J., M. B. Bishop, and V. Taylor (1995a), All-sky measurements of short period waves imaged in the OI(557. 7 nm), Na(589. 2 nm) and near-infrared OH and $O_2$(0,1) nightglow emissions during the ALOHA-93 campaign, *Geophys. Res. Lett.*, *22*, 2833–2836.

Taylor, M. J., D. N. Turnbull, and R. P. Lowe (1995b), Spectrometric and imaging measurements of a spectacular gravity wave event observed during the ALOHA-93 campaign, *Geophys. Res. Lett.*, *22*, 2849–2852.

Tricker, R. A. R. (1965), *Bores, Breakers, Waves and Wakes*, 250 pp, Elsevier, New York.

Wu, Q., and T. L. Killeen (1996), Seasonal dependence of mesospheric gravity waves (<100 km) at Peach Mountain Observatory, Michigan, *Geophys. Res. Lett.*, *23*, 2211–2214.

Yamada, Y., H. Fukunishi, T. Nakamura, and T. Tsuda (2001), Breaking of small-scale gravity wave and transition to turbulence observed in OH airglow, *Geophys. Res. Lett.*, *28*, 2153–2156.

J. Baumgardner, M. Mendillo, and S. M. Smith, Center for Space Physics, Boston University, 725 Commonwealth Avenue, Boston, MA 02215, USA. (smsm@bu.edu)

E. R. Reisin and J. Scheer, Instituto de Astronomía y Física del Espacio, CONICET, UBA, Ciudad Universitaria, C.C.67, Suc. 28, 1428 Buenos Aires, Argentina.